World Journal of Engineering and Technology, 2017, 5, 105-116
http://www.scirp.org/journal/wjet
ISSN Online: 2331-4249
ISSN Print: 2331-4222

# Aerodynamics and Flight Dynamics of Free-Falling Ash Seeds

**Rui Fang[1], Yanlai Zhang[1], Yanpeng Liu[2]**

[1]School of Transportation Science and Engineering, Beihang University, Beijing, China
[2]School of Aeronautic Science and Engineering, Beihang University, Beijing, China
Email: yanpengliu@buaa.edu.cn

**How to cite this paper:** Fang, R., Zhang, Y.L. and Liu, Y.P. (2017) Aerodynamics and Flight Dynamics of Free-Falling Ash Seeds. *World Journal of Engineering and Technology*, **5**, 105-116.
https://doi.org/10.4236/wjet.2017.54B012

**Received:** September 20, 2017
**Accepted:** October 9, 2017
**Published:** October 12, 2017

## Abstract

Samaras or winged seeds spread themselves by wind. Ash seed, unlike other samaras, has a high aspect ratio wing which can generate enough lift force to slow down descent by rotating about the vertical axis and spinning around its wing span axis simultaneously. This unique kinematics and inherent fluid mechanism are definitely of great interest. Detailed kinematics of free falling ash seeds were measured using high-speed cameras, then corresponding aerodynamic forces and moments were calculated employing computational fluid dynamics. The results show that both rotating and spinning directions are in the same side and the spinning angular velocity is about 6 times of rotating speed. The terminal descending velocity and cone angles are similar to other samaras. Analysis of the forces and moments shows that the lift is enough to balance the weight and the vertical rotation results from a processional motion of total angular moment because the spin-cycle-averaged aerodynamic moment is perpendicular to the total angular moment and can only change its direction but maintain its magnitude, which is very similar to a spinning top in processional motion except that the total angular moment of ash seed is not along the spin axis but almost normal to it. The flow structures show that both leading and trailing edge vortices contribute to lift generation and the spanwise spinning results in an augmentation of the lift, implying that ash seeds with high aspect ratio wing may evolve in a different way in utilizing fluid mechanisms to facilitate dispersal.

## Keywords

Ash Seed, Kinematics Measurement, Aerodynamics, Leading Edge Vortex, Trailing Edge Vortex

## 1. Introduction

There are two kinds of seeds that dispersed by wind, pappose seeds (parachute type) and winged seeds. Pappose seeds utilized rag force acting on the pappi [1], while winged seeds mainly use lift force on their wings [2].The dispersal of winged seeds can be divided into two categories according to the locations of their center of gravity. When located in front of the seed's aerodynamic center, the seed exhibits a glider type translation during fall, without any rotation [3]. However, if located near the terminal end of the wing, *i.e.*, maple and ash seeds, they all inevitably experience rotation during fall. It is the main mechanism behind their long-distance dispersal success, though their wing loading can be 450% higher than that of gliding and straying seeds as found by D. Lentink [4]. Such high aerodynamic performance may have wide applications in engineering as well, particularly in the design of helicopters and new concept aerial vehicles [5].

The aerodynamic characteristics of autorotating seeds have been investigated theoretically and experimentally [6] [7]. At the beginning, researchers mainly focused on the relationship between their aerodynamic performance and geometrical configurations [8] [9]. Various autorotating seeds have been experimentally tested to determine the relationship between wing-loading and flight characteristics, such as descent and rotational angular velocities.

Recently, with the rapid development of measurement techniques and equipment, e.g., stereoscopic PIV (Particle Image Velocimetry), tomographic PIV and high-speed cameras, detailed flow field measurement around a rapidly autorotating seed became feasible [10]. Researchers found the slow decent maple seeds unexpectedly utilize an unusual high lift mechanism, Leading-Edge Vortex (LEV), which had been proved be widely used by the flapping wings of the insects [11] and other flying creatures [12]. In both cases, the existence of a strong span wise flow on the geometrical upper surface is responsible for the stable attachment of the LEV. Besides the winged seeds that rotate about the vertical axis like many different kinds of maple seed, there is another class of winged seeds, such as ash seed and tulip seed, which are rotating about the vertical axis and spinning around the wing span axis simultaneously during free falling [5]. Such unique autorotation is due to: 1) their mass is nearly symmetrically distributed with respect to the wing span axis; 2) their wing usually has a relative high aspect ratio. So far, detailed study of this biaxial autorotation is rare. Consequently, its aerodynamics and kinematics are still poorly understood.

In this paper, aerodynamics and kinematics of free-falling ash seeds were investigated by means of experimental measurement and computational fluid dynamics. Morphological and kinematical data of stable autorotating and descending seed were measured with high temporal-spatial accuracies, following by numerical simulation based on the measured data; hence, the instantaneous flow field induced by the seed was fully resolved. As a whole, numerical results show several distinct flow structure features and their evolving tendencies, which give clear clues in understanding the essences of such unique autorotation, including the force balance, lift mechanism and the coupling between aerodynamic force and kinematics response.

## 2. Experimental Apparatus and Methods

### 2.1. Seeds

Ash is common English name for *Fraxinus* genus plants tree, which is widespread across much of Europe, Asia and North America, often planted as shade tree. The seeds used in this paper were collected from the botanical garden of Institute of Botany, Chinese Academy of Sciences, and preserved in sealed bags to keep moisture. Eleven seeds that successfully enter the terminal stable autorotating and descending state in experiment trials were selected for further measurement and analysis. A typical sample of ash seed is shown in **Figure 1**.

As shown in **Figure 1**, ash seed exhibit a nearly symmetrical structure relative to the wingspan axis. Each sample seed's mass was measured with an electronic balance with accuracy of 0.01 mg. The planer shape of these seeds was acquired using a scanner, thus the length, chord length and area of the winged seed can be obtained easily. **Table 1** summarizes the morphological and kinematical parameters of all eleven ash seeds used.

### 2.2. Experimental Apparatus

A schematic diagram of the experimental apparatus is shown in **Figure 2**. Seeds were released ~2 m above the floor, which is high enough for the seeds to reach the stable terminal state. The observation section is surrounded by transparent and diffusive films to avoid any ambient disturbances. Also, diffusive films opposite


**Figure 1.** A typical ash seed.

**Table 1.** Morphological and kinematics parameters of ash seeds.

| Parameter | Value ± STD |
|---|---|
| mass (mg) | 26.4 ± 1.6 |
| Total wingspan (mm) | 44.2 ± 2.0 |
| Wing area (mm²) | 156.0 ± 14.4 |
| Wing loading (N/mm²) | 1.67 ± 0.11 |
| Mean chord length (mm) | 3.53 ± 0.20 |
| Turn radius (mm) | 28.5 ± 1.97 |
| Descending velocity (mm/s) | 1114.2 ± 71.2 |
| Angular velocity about vertical axis (rad/s) | 61.5 ± 3.4 |
| Angular velocity around wing span axis (rad/s) | 380.0 ± 23.7 |
| Coning angle (degree) | 25.3 ± 4.2 |


**Figure 2.** Experimental apparatus.

to the front and side cameras also make the backlit LED light sources (not shown in **Figure 2** for the purpose of clarity) as even as possible. In order to clearly tell the rotating and spinning direction and correctly measure their angular velocities, three high-speed cameras were placed orthogonally and used to record the falling seed from the front, the side and the upwards directions, respectively. Each camera's field of view (FOV) is about 40 × 20 cm, enough to cover several intact cycles of falling seeds based on their terminal descending speed as given in **Table 1**.

## 3. Computational Method

Using the experimental results as kinematic input for numerical simulation, it is possible to further identify the aerodynamic characteristics of the falling seeds, and find the mechanical mechanism from the perspective of lift generation and flow field. This section describes the computational fluid dynamics method and mesh models used and performs independence verification of some of mesh parameters.

### 3.1. Governing Equations and the Solution Method

The governing equations of the flow around the flapping and rotary wings are the 3D incompressible unstable Navier-Stokes equations. The artificial compressibility method developed by Rogers [13] is used to solve the velocity and pressure. The governing equations in the curvilinear coordinate system are written as follows:

$$\frac{\partial \hat{\boldsymbol{Q}}}{\partial \tau} = -\frac{\partial}{\partial \xi}\left(\hat{\boldsymbol{E}} - \hat{\boldsymbol{E}}_v\right) - \frac{\partial}{\partial \boldsymbol{\eta}}\left(\hat{\boldsymbol{F}} - \hat{\boldsymbol{F}}_v\right) - \frac{\partial}{\partial \zeta}\left(\hat{\boldsymbol{G}} - \hat{\boldsymbol{G}}_v\right) + \boldsymbol{H}_{GCL} \tag{1}$$

where $\hat{\boldsymbol{Q}} = 1/J\left[p \;\; u \;\; v \;\; w\right]^T$ is the primitive variables, and $J$ is the Jacobian determinant between the Cartesian coordinate system and the curvilinear coordinate system with the transformations $\xi = \xi(x, y, z, t)$, $\eta = \eta(x, y, z, t)$, $\zeta = \zeta(x, y, z, t)$ and $\tau = t$. The symbols $\hat{\boldsymbol{E}} = \left(\hat{\boldsymbol{F}} \text{ and } \hat{\boldsymbol{G}}\right)$ and $\hat{\boldsymbol{E}}_v = \left(\hat{\boldsymbol{F}}_v \text{ and } \hat{\boldsymbol{G}}_v\right)$ are the convective and viscous fluxes respectively. In the viscous fluxes, $Re$ is defined as u $Re = \bar{u}c/\nu$ where $\bar{u}$ is the reference velocity, which is defined as the mean velocity of seed tip, $c$ is the chord length, and $\nu$ is the kinematic viscosity of fluid. For a moving/deforming mesh, the term $\boldsymbol{H}_{GCL}$ is added to the right side of Equation (1) to enforce the geometric conservation law. A pseudo-time derivative of pressure is introduced into the continuity equation to solve Equation (1). This derivative uses the third-order flux-difference splitting technique for convective terms and the second-order central-difference scheme for viscous terms. The time derivatives in the momentum equation are computed using a three-point backward-difference implicit formula. Arithmetic accuracy is in second order for space and time.

Once the fluid field is solved numerically, integrating the pressure and viscous stress over the wing surface provides the total aerodynamic force acting on the wing. The vertical component of the total force is referred to as lift $L$, and the moment generated by the force component in the direction of the rotation is referred to as rotating moment $Q$. The dimensionless lift and rotating moment are referred to as lift $C_L$ and rotating moment $C_Q$ coefficients:

$$C_L = \frac{L}{0.5\rho(\bar{u})^2 S} \tag{2}$$

$$C_Q = \frac{Q}{0.5\rho(\bar{u})^2 Sc} \tag{3}$$

where $\rho$ is the air density and $S$ is the wing area.

### 3.2. Mesh Model and Validation

An O-H type mesh is used for numerical simulation (**Figure 3**). Before studying the aerodynamic forces and flow field of the wing model, CFD code [14], mesh density, the first mesh spacing, computation time step, and computational domain size used in this study have been validated, as shown in **Figure 4**, here, the time $\hat{t}$ is non-dimensionalized by the period of spinning around wing span axis. As a result, a numerical solution independent of mesh and time steps can be achieved when the mesh dimension is 70 × 75 × 152 (in the normal, chordwise, and spanwise directions, respectively), the domain size is 30c, the first mesh spacing at the wall is 0.001c, and 400 time steps are used in one spinning cycle.

## 4. Results and Discussion

Eleven free falling trails in stable autorotation were filmed successfully. For each trail, about 3 whole cycles of rotation around vertical axis were recorded and digitalized to obtain all kinematics parameters needed. As an example, snapshoots of one seed in free falling are overlapped and given in **Figure 5** in every 15, 10, 5 and 1 frames, respectively.

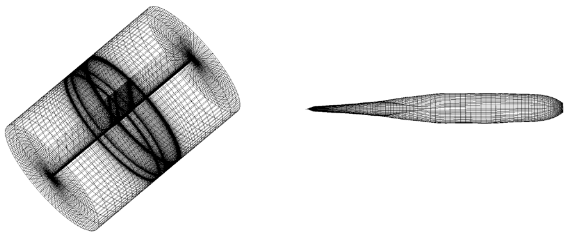


**Figure 3.** Computational mesh: (a) Overall; (b) Wing surface.

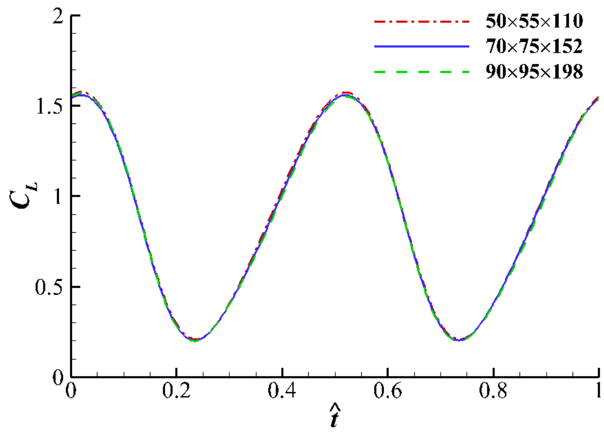


**Figure 4.** Mesh-independence validation.

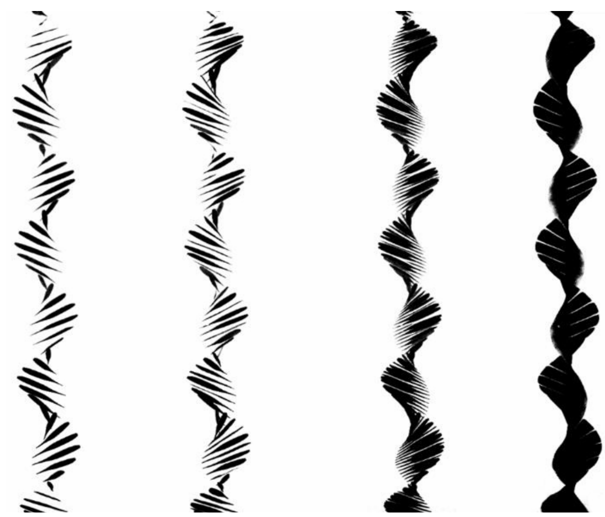

**Figure 5.** Superimposed images of a falling ash seed.

## 4.1. Kinematic and Morphological Parameters of Free Falling Ash Seeds

To describe wing kinematics, two coordinate systems are introduced here (see **Figure 6**), the earth frame (*oxyz*) and the wing-fixed frame ($ox_w y_w z_w$). The $z_w$ axis is along wing span and the $x_w$ axis is along the chord line pointing to leading edge. The kinematic parameters are the descending velocity ($v_d$), rotational speed about vertical axis ($\omega$), spinning speed around wing span axis ($\omega_f$) and

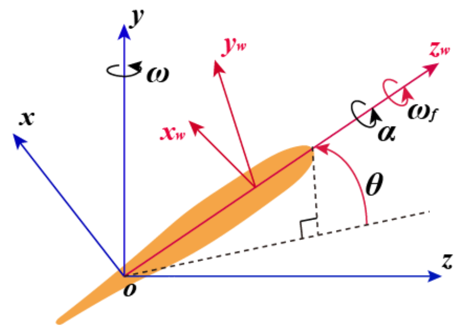


**Figure 6.** Definitions of the frames of reference.

coning angle ($\theta$). The coning angle ($\theta$) is defined as the angle between the wing span axis ($z_w$) and the horizontal plane ($xz$), the pitch angle ($\alpha$) is the angle between the chord line of the seed ($x_w z_w$) and the horizontal plane ($xz$). **Table 1** gives the kinematic and morphological parameters.

## 4.2. Aerodynamic Forces and Moments

The time history of the lift coefficient is shown in **Figure 7(a)**. The periodical lift shows that the ash seed reaches a stable state and experiences two times variations of lift within one spin cycle. When the upward surface flips downward, the lift varies in a period. It can also be seen that the time course of lift is similar to a sinusoid curve and the peak $C_L$ reaches about 1.5. The cycle-averaged lift coefficient ($C_{Lavg}$ = 0.889) is about 10% larger than the seed non-dimensional weight ($G^* = mg / 0.5\rho\left(\bar{u}\right)^2 S = 0.806$), which indicates that the seed weight is balanced by the aerodynamic force pretty well, enabling the ash seed to descend at a relative low speed (see **Table 1**, $v_d$ = 1.114 m/s).

**Figure 7(b)** presents the aerodynamic moment about the vertical axis. Although the maximum and minimum moment in one span spinning cycle are not symmetric about zero, the cycle-averaged moment is very close to zero, implying that rotating about vertical axis also reach a stable state. When the wing surface rotates from horizontal to vertical, the moment direction is opposite to the vertical rotation, which works as a drag preventing the rotation; while the wing surface flips from vertical to horizontal, the moment direction is same as the vertical rotation, indicating that the wing aerodynamic force plays a role of thrust driving the wing to rotate. Overall, the moment driving the wing to rotate around the vertical axis is generated when the wing surface flip from vertical to horizontal, while the damping moment is generated when the wing surface flip from horizontal to vertical.

**Figure 8** gives the contour plot of vorticity at span location of 60% wing length from wing root. At time $t_1$, the wing generates maximum lift and the leading-edge vortex (LEV) is formed and remains attached to its upper surface, while the trailing edge vortex is also quite strong but separates from the wing surface. At time $t_2$, the wing pitches up and the LEV starts to separate from the wing surface, correlating with a dramatic decrease in lift. When the wing pitches

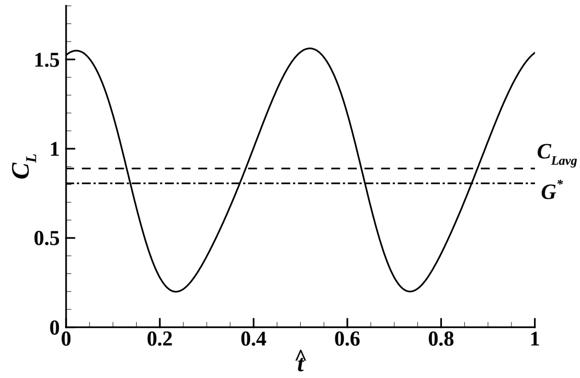


(a)

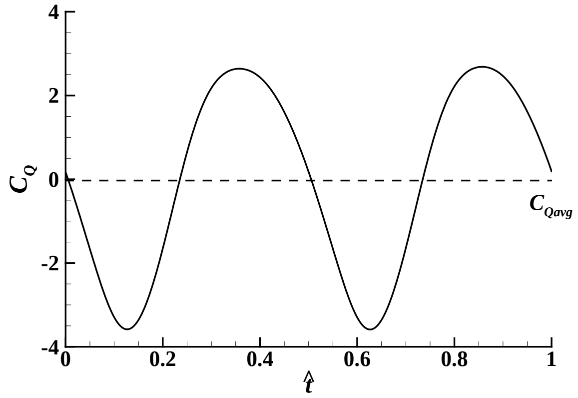


(b)

**Figure 7.** (a) Time history of lift coefficient in one spinning period; (b) Moment coefficient about the vertical axis.

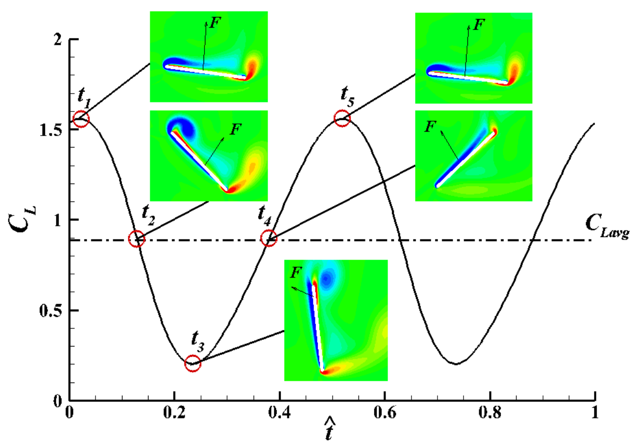


**Figure 8.** Vorticity plot at span location of 60% wing length from the wing root.

almost upright ( $\alpha = 84^\circ$ ), the lift decreases to its minimum value. It is obvious that from $t_1$ to $t_3$ the horizontal component of aerodynamic force ($F$) is drag, meaning its direction is opposite to rotating motion. On the other hand, while from $t_3$ to $t_5$the horizontal component of aero dynamic force is thrust. As a result, the cycle-averaged moment $C_{\text{Qavg}}$ is almost zero due to its periodical essence.

### 4.3. Dynamical Equilibrium of Free Falling Motion

As aforementioned, due to rotations about vertical axis and span axis, the seed can generate enough aerodynamic force to balance its weight, which allowing a low speed descent. However, the lift is not through the center of mass, therefore there exist aerodynamic moments acting on the mass of center. To explain this, another frame ( $ox'y'z'$ ) has to be introduced, whose $z'$ axis is in the same direction as the $z_w$ axis and $x'$ axis always in horizontal, thus the frame ( $ox'y'z'$ ) only rotates about $y$ axis as the wing rotates. As a result, the spin-cycle-averaged aerodynamic moment will be parallel to $x'$ axis. And the spin-cycle-averaged total angular moment ( $\boldsymbol{L}$ ) will be in $oy'z'$ plane (see **Figure 9**), which can be determined as:

$$\boldsymbol{L} = I_z(\boldsymbol{\omega}_1 + \boldsymbol{\omega}_f) + I_y\boldsymbol{\omega}_2 \quad (4)$$

where $I_y$ and $I_z$ are moment of inertia about $y'$ and $z'$, $\omega_1$ and $\omega_2$ are the components of $\omega$ in $z'$ and $y'$, $\omega_f$ is the Euler angle rate ( $\dot{\alpha}$ ) about $z'$. Therefore, the $z'$ component of angular moment ( $\boldsymbol{L}_1 = I_z(\boldsymbol{\omega}_1 + \boldsymbol{\omega}_f)$ ) is much smaller than that of $y'$ component of angular moment ( $\boldsymbol{L}_2 = I_y\boldsymbol{\omega}_2$ ), because $I_y$ is about two order larger than $I_z$ while $\omega_1$, $\omega_2$ and $\omega_f$ in same order. Therefore, the total angular moment ( $\boldsymbol{L}$ ) is almost perpendicular to axis $z'$ in $oy'z'$ plane (see **Figure 9**). It should be noticed that the cycle-averaged moment due to aerodynamic forces is perpendicular to the total angular moment (the averaged moment about $y$ axis nearly zero, see **Figure 7(b)**), thus only driving the total angular moment vector to process (rotating about vertical axis $y$ ) but not change its magnitude. It can also be seen that the time rate of cycle-averaged total angular moment is:

$$\mathrm{d}\boldsymbol{L}/\mathrm{d}t = \boldsymbol{\omega} \times \boldsymbol{L} \quad (5)$$

which is pointing to the same direction of the aerodynamic moment. This processional movement about vertical axis is very similar to the processional movement of a spinning top on a table whose moment is caused by gravity, except that the total angular moment of ash seed is not along the spin axis but almost normal to it (**Figure 9**).

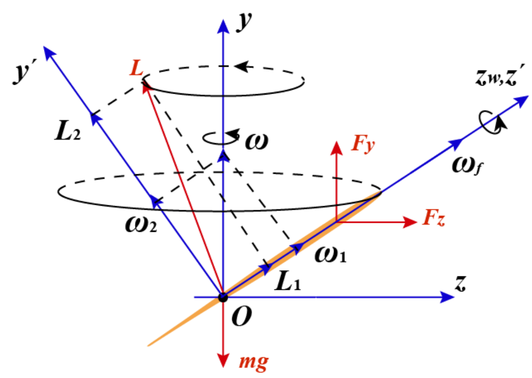


**Figure 9.** Schematic sketch of forces, moments and angular moments.

### 4.4. Near Field Flow Structure and Wing Surface Pressure Distribution

The contour plots of $z_w$ component of vorticity at different spanwise position from non-dimensional time $t_1$ to $t_4$ are given in **Figure 10**, as well as wing surface pressure distributions. It can be seen that, at time $t_1$,from wing root to tip, the LEV remains attached, therefore a lower pressure occurs on the upper surface near leading edge; at time $t_2$, as the wing spins, the LEV and TEV are all detached, the lower pressure on the upper surface increases, correlating with a decrease in aerodynamic force; at time $t_3$, the pressures of both surfaces become almost same, thus a lowest force is generated; at time $t_4$, the pressure of upper surface are not as much lower as that at time $t_1$ but it covers a relative large region, and the pressure of lower surface also becomes more smoother, thereby generating almost same forces as time $t_2$.

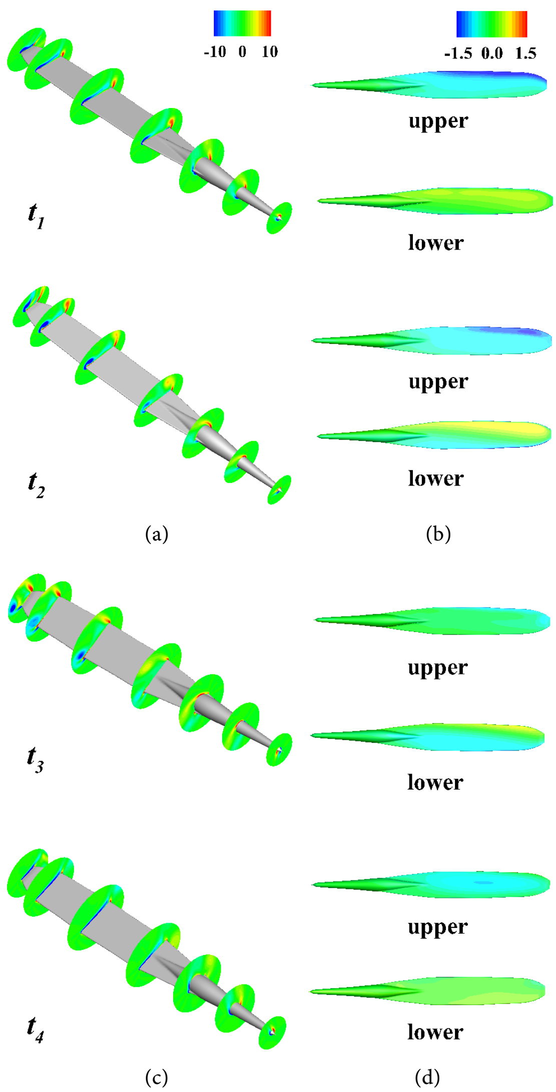


**Figure 10.** The contour plots of $z_w$ component of vorticity and wing surface pressure at different times. (a) and (c): Vorticity; (b) and (d): Wing surface pressure distribution.

## 5. Conclusion

Detailed kinematics of free falling ash seeds were measured using high-speed cameras, then corresponding aerodynamic forces and moments were calculated employing computational fluid dynamics. The results show that both rotating and spinning directions are in the same side and the spinning angular velocity is about 6 times of the rotating speed. The terminal descending velocity and cone angles are similar to other samaras. Analysis of the forces and moments shows that the lift is enough to balance the weight and the vertical rotation results from a processional motion of total angular moment because the spin-cycle-averaged aerodynamic moment is perpendicular to the total angular moment and can only change its direction but maintain its magnitude, which is very similar to a spinning top in processional motion except that the total angular moment of ash seed is not along the spin axis but almost normal to it. The flow structures show that both leading and trailing edge vortices contribute to lift generation and the spanwise spinning results in an augmentation of the lift, implying that ash seeds with high aspect ratio wing may evolve in a different way in utilizing fluid mechanisms to facilitate dispersal.

## Acknowledgements

This research was primarily supported by the National Natural Science Foundation of China (No. 11672028).

## References

[1] Greene, D.F. and Johnson, E.A. (1990) The Aerodynamics of Plumed Seeds. *Functionas Ecology*, **4**, 117-125. https://doi.org/10.2307/2389661

[2] Nathan, R. (2006) Long-Distance Dispersal of Plants. *Science*, **313**, 786-788. https://doi.org/10.1126/science.1124975

[3] Azuma, A. and Okuno, Y. (1987) Flight of a Samara, *Alsomitra macrocarpa*. *Journal of Theoretical Biology*, **129**, 263-274. https://doi.org/10.1016/S0022-5193(87)80001-2

[4] Lentink, D., Dickson, W.B., van Leeuwen, J.L. and Dickinson, M.H. (2009) Leading-Edge Vortices Elevate Lift of Autorotating Plant Seeds. *Science*, **324**, 1438-1440. https://doi.org/10.1126/science.1174196

[5] Sirohi, J. (2013) Microflyers: Inspiration from Nature. *Proceedings of SPIE—The International Society for Optical Engineering*, **8686**, 1-15. https://doi.org/10.1117/12.2011783

[6] Azuma, A. and Yasuda, K. (1989) Flight Performance of Rotary Seeds. *Journal of Theoretical Biology*, **138**, 23-53. https://doi.org/10.1016/S0022-5193(89)80176-6

[7] Yasuda, K. and Azuma, A. (1997) The Autorotation Boundary in the Flight of Samaras. *Journal of Theoretical Biology*, **185**, 313-320. https://doi.org/10.1006/jtbi.1996.0299

[8] Peroni, P.A. (1994) Seed Size and Dispersal Potential of Acer Rubrum (Aceraceae) Samaras Produced by Populations in Early and Late Successional Environments. *American Journal of Botany*, **81**, 1428-1434. https://doi.org/10.2307/2445316

[9] Greene, D.F. and Johnson, E.A. (1993) Seed Mass and Dispersal Capacity in

Wind-Dispersal Diaspores. *Oikos*, **67**, 69-74. https://doi.org/10.2307/3545096

[10] Salcedo, E., Treviño, C., Vargas, R.O. and Martínez-Suástegui, L. (2013) Stereoscopic Particle Image Velocimetry Measurements of the Three-Dimensional Flow Field of a Descending Autorotating Mahogany seed (*Swietenia macrophylla*). *The Journal of Experimental Biology*, **216**, 2017-2030. https://doi.org/10.1242/jeb.085407

[11] Ellington, C.P., van den Berg, C., Willmott, A.P. and Thomas, A.L.R. (1996) Leading-Edge Vortices in Insect Flight. *Nature*, **384**, 626-630. https://doi.org/10.1038/384626a0

[12] Birch, J.M. (2004) Force Production and Flow Structure of the Leading Edge Vortex on Flapping Wings at High and Low Reynolds Numbers. *Journal of Experimental Biology*, **207**, 1063-1072. https://doi.org/10.1242/jeb.00848

[13] Rogers, S.E., Kwak, D. and Kiris, C. (1991) Stable and Unstable Solutions of the Incompressible Navier-Stokes Equations. *AIAA Journal*, **29**, 603-610. https://doi.org/10.2514/3.10627

[14] Wu, J., Wang, D. and Zhang, Y. (2015) Effects of Kinematics on Aerodynamic Periodicity for a Periodically Plunging Airfoil. *Theoretical and Computational Fluid Dynamics*, **29**, 433-454. https://doi.org/10.1007/s00162-015-0366-5